



Experimental Investigation of the Effects of Subgrade Strength and Geogrid Location on the Cyclic Response of Geogrid-Reinforced Ballast

Romarc Léo Esteban Desbrousses¹ · Mohamed A. Meguid¹ · Sam Bhat²

Received: 15 May 2023 / Accepted: 29 August 2023 / Published online: 27 September 2023
© The Author(s), under exclusive licence to Springer Nature Switzerland AG 2023

Abstract

This study aims to investigate how the subgrade strength and the location of a geogrid within a ballast layer affect the geosynthetic's ability to stabilize railroad ballast. To do so, a total of thirteen large-scale cyclic load tests are performed on unreinforced tie-ballast assemblies and on tie-ballast assemblies reinforced with a geogrid placed at a depth of 150 mm, 200 mm, and 250 mm to compare the mechanical behavior of unreinforced ballast with that of geogrid-reinforced ballast. The results suggest that the compressibility of the subgrade supporting a geogrid-reinforced tie-ballast assembly plays a crucial role in determining the geogrid's reinforcing efficiency. In cases where a geogrid-reinforced ballast layer is supported by a competent subgrade, the geogrid's performance appears insensitive to its placement depth. However, the geogrid's location yields an increasingly significant influence over its ability to stabilize railroad ballast as the underlying subgrade becomes softer, with geogrids placed closer to the loaded area outperforming those located deeper in the ballast layer. The inclusion of geogrids in railroad ballast leads to reductions in the tie's permanent and resilient settlement which vary depending on the geogrid's location and subgrade compressibility. However, the tie-ballast assemblies' damping ratio appears to be insensitive to the presence of geogrids.

Keywords Ballast · Subgrade · Geogrid · Tie settlement · Cyclic loading · Ballast box test

Introduction

The stability of ballasted railroad tracks depends to a great degree on the performance of the ballasted track structure that supports train traffic [1]. A ballasted track structure may be divided into a superstructure that comprises the rail-tie assembly and an underlying multi-layer geotechnical system called the substructure which is composed of the ballast, sub-ballast, and subgrade layers and provides a bearing

platform on which the superstructure rests, thereby playing a crucial role in preserving the level of track alignment required to maintain safe track riding conditions.

The ballast layer is the uppermost stratum in the substructure and consists of an unbound assembly of hard, angular, crushed rocks. Its primary functions include supporting traffic-induced loads while safely transferring them down to the underlying soil layers, maintaining satisfactory horizontal and vertical track alignment, and providing ample void space to allow for fast drainage and accommodate the presence of fine materials in the layer [2–6]. As it is located directly beneath the ties, the ballast layer is exposed to high dynamic loads that are responsible for the development of considerable non-recoverable deformations in the layer, making it one of the main sources of settlement in ballasted railway tracks.

The deformations that arise in the ballast layer are governed by the material's unbound and discrete nature, its generally low levels of lateral confinement, and the train loads it is subjected to. At the onset of cyclic loading in newly laid tracks, the loosely packed ballast aggregate coupled with the absence of appreciable lateral confinement

✉ Romarc Léo Esteban Desbrousses
romarc.desbrousses@mail.mcgill.ca

Mohamed A. Meguid
mohamed.meguid@mcgill.ca

Sam Bhat
sam@titanenviro.ca

¹ Department of Civil Engineering, McGill University, 817 Sherbrooke St. W., Montreal, QC H3A 0C3, Canada

² Titan Environmental Containment Ltd., 777 Quest Blvd, Ile des Chenes, MB R0A 0T1, Canada

foster conditions that are conducive to a rapid buildup of non-recoverable vertical and lateral deformations in the ballast layer as individual ballast particles move and slide past another to rearrange into a more stable and denser packing in response to the repeated application of train loads [7–14]. The densification of the ballast layer leads to the formation of a strong interlock between the ballast particles that are now tightly wedged against each other, resulting in an increase in the layer's stiffness and a reduction in the rate at which settlement accumulates under further cyclic loading as the granular assembly behaves almost elastically during loading–unloading cycles.

Over time and due to sustained exposure to cyclic train loading, the ballast aggregate degrades and individual particles break down into finer ones. This generation of smaller particles contributes to the progressive filling of the void space in the layer in a process known as fouling. Fouled ballast possesses a lower shear strength and poorer drainage capabilities compared to fresh ballast and as such is prone to accumulating settlement at an increasing rate when subjected to cyclic train loading, potentially leading to even more subsidence, particularly in cases where the subgrade is made of fine-grained soils with low shear strength and high plasticity that are vulnerable to developing large deformations under cyclic loading [15–17].

The development of excessive deformations in the ballast layer has an adverse effect on the track alignment and leads to a degradation in track safety and riding quality. This usually prompts either the imposition of speed limits on affected track sections or the scheduling of costly periodic ballast maintenance operations such as tamping or stone-blowing to correct track alignment issues [18–20]. Tamping is the most common ballast maintenance operation and consists of lifting the ties while inserting tamping tines into the ballast layer to simultaneously squeeze and vibrate the aggregate under the ties to restore an acceptable track level. Although this method is initially effective at correcting track geometry issues, its benefits are offset by the fact that it loosens, disturbs, and damages the ballast material which typically experiences a period of rapid settlement accumulation following the resumption of train traffic [21, 22]. On the other hand, stone-blowing is an alternative to tamping whereby the ties are lifted while a set volume of gravel is pneumatically injected under the ties. Since stone-blowing does not disturb the underlying ballast bed, only minor deformations occur once train traffic resumes on affected track sections [20, 22]. Given the elevated cost of maintenance operations, alternatives, such as the inclusion of geogrid reinforcement in the ballast layer, are being used to improve the in-service performance of railroad ballast and curtail its operating costs [1, 23–25].

A geogrid is used to reinforce ballast, thanks to its ability to develop a strong mechanical interlock with the surrounding

particulate matter, forming a semi-rigid mat that laterally confines the granular assembly to minimize its deformations [26]. The performance of a geogrid embedded in railroad ballast is a function of its aperture size, its placement depth, and the compressibility of the underlying subgrade soil. The size of a geogrid's apertures (A) in comparison with that of the surrounding soil particles, generally represented by the mean particle diameter (D_{50}), must be sufficiently large to allow the ballast particles to strike through its plane for a strong interlock to form. Experiments conducted on geogrid-reinforced ballast have indicated that an optimal interlock is achieved with an A/D_{50} ratio of 0.95–1.20 while A/D_{50} ratios in excess of 1.20 yield adequate reinforcement [27–34].

Similarly, large-scale cyclic loading experiments performed on geogrid-reinforced ballast samples have demonstrated that a geogrid is more effective at stabilizing railroad ballast when placed closer to the bottom of the ties [35–37]. However, a geogrid must also be placed sufficiently deep within the ballast bed so as not to interfere with potential ballast operations that generally affect the layer's upper 100–150 mm. This has led to the recommendation that geogrids should be placed at least 150 mm below the base of the ties. Additionally, experimental and numerical modeling works on geogrid-reinforced ballast have highlighted that the strength of the subgrade supporting a reinforced ballasted substructure wields a considerable influence over the type of benefit derived from reinforcing ballast with geogrids, with geogrids being reported to be more effective at reducing track settlement in tracks supported by weak subgrades [36–38]. However, most experimental studies conducted to date have been limited to comparing the behavior of geogrid-reinforced ballast samples supported by a stiff subgrade to a soft subgrade without capturing how different subgrade strengths affect the performance of geogrid-reinforced ballast.

As such, this paper focuses on studying the relationship between the performance of a geogrid embedded in a ballast layer, its placement depth, and the strength of the underlying subgrade. To do so, a series of large-scale ballast box tests is performed on unreinforced and geogrid-reinforced tie–ballast assemblies resting on different subgrades to compare the behavior of railroad ballast under various conditions and capture its sensitivity to the presence of geogrid reinforcement. The parameters monitored during the experiments include the tie's permanent settlement, its resilient deflection, the tie support stiffness, and the ballast's damping ratio.

Methodology

Materials

Ballast

Crushed granite aggregate quarried in St-Hippolyte, Quebec (Canada) screened to conform with an AREMA No. 4 grading (see Fig. 1) typical of mainline ballast material is used in the experiments presented in this paper. The aggregate’s physical properties are summarized in Table 1 and conform with the relevant recommended limiting values for ballast material outlined in AREMA’s *Manual for Railway Engineering* [39]. In every experiment, a new 300 mm-thick layer of railroad ballast is constructed in the ballast box in three 100 mm-thick lifts compacted to a target unit weight of 15.7 kN/m³ using an Exen EKCA handheld vibrating plate compactor. The compactor applies a 30.1 kgf over a 120×150 mm area at a frequency of 133 Hz. The compactor is passed over six 150 mm-wide strips running in the direction of the 1290 mm-long side of the box for 30 s on each strip, resulting in a total compaction time of 3 min per lift. A ballast thickness of 300 mm is chosen to reflect the typical depth of ballast layers in standard gage tracks in North America [39].

Geogrid

In the reinforced ballast box tests, ballast layers are reinforced with a biaxial polypropylene geogrid designed to stabilize ballast aggregate in railroad applications. The geogrid is manufactured such that it possesses thick integral

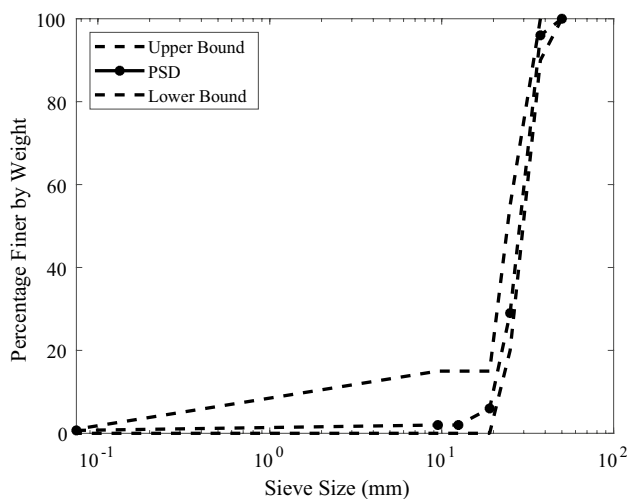


Fig. 1 Particle size distribution of the granite aggregate used in the ballast box tests (AREMA No. 4)

Table 1 Properties of the crushed granite aggregate

Properties	Value
Flat and elongated particles (ASTM D4791)	0%
Flat particles (ASTM D4791)	3%
Los Angeles abrasion (ASTM C535)	32.8%
Dry bulk specific gravity (ASTM C127)	2.741
Loose bulk density (ASTM C29)	1400 kg/m ³
Compacted bulk density (ASTM C29)	1600 kg/m ³

nodes, thick ribs, and large square apertures to allow for the development of a strong mechanical interlock with the surrounding coarse ballast aggregate. The geogrid’s physical and the mechanical properties are summarized in Table 2 [40, 41]. A new geogrid sheet is used for every reinforced ballast box test. To prevent the geogrid from warping around the edges of the box, every sheet is trimmed to a size of 700×1030 mm.

Artificial Subgrades

To simulate the presence of different subgrades below the ballast layer and capture their effect on the tie’s settlement, the box’s bottom steel plate is covered with one of three assortments of elastomer pads each with its own compressibility. The compressibility of each rubber mat combination is expressed as an equivalent soil strength by performing a California Bearing Ratio (CBR) test on the mats following the procedure outlined in ASTM D1883 [42]. The three artificial subgrades used in this study have CBR readings of 25, 13, and 5 and are herein referred to as the competent, fair, and soft subgrades respectively while the condition where the box’s bottom steel plate alone is used to provide a bearing platform to the overlying ballast layer is referred to as the stiff subgrade. The properties of each artificial subgrade are summarized in Table 3.

Experimental Setup

A series of ballast box tests is conducted by constructing 300 mm-thick ballast layers in a ballast box with plan dimensions of 915×1290 mm and a depth of 600 mm (see Fig. 2).

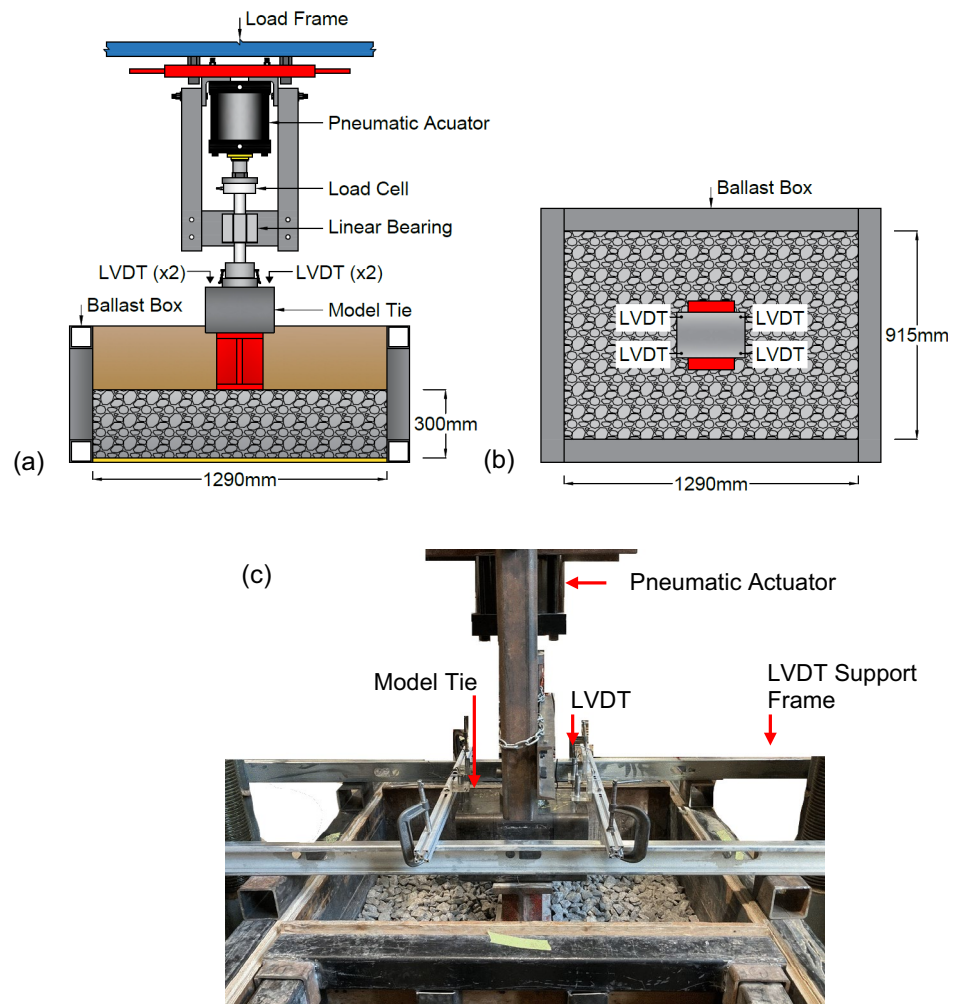
Table 2 Physical and mechanical properties of the biaxial geogrid [40, 41]

Aperture size (mm)	Ribs/m	Rib thickness (mm)	Tensile strength (kN/m)		
			Ultimate	5% Strain	2% Strain
57/57	17	1.8/1.2	30/30	21/21	11/11

Properties are reported as minimum average roll values (MARV) in the machine direction/cross-machine direction

Table 3 Rubber mat properties

Subgrade	Stiff	Competent	Fair	Soft
CBR	∞	25	13	5
Material	Steel plate	12.7 mm-thick 60A neoprene rubber mat	12.7 mm-thick 40A neoprene rubber mat	12.7 mm-thick 40A neoprene rubber mat + 25.4 mm-thick 60A neoprene rubber mat

Fig. 2 **a** pneumatic cyclic loading apparatus and its ballast box, **b** plan view of the ballast box, **c** laboratory set up

The ballast box consists of an outer rigid frame composed of welded hollow steel sections that create a central enclosure lined on the edges with 38 mm-thick plywood sheets covered with smooth sheet metal fixed to the outer frame and a steel plate at the bottom. Upon placing and compacting the ballast sample in the ballast box, a model tie consisting of a steel I-beam with plan dimensions of 301×203 mm and a hollow steel section bolted to its top is placed above the 300 mm-deep ballast bed to transmit the desired cyclic compressive loads to the granular assembly.

The ballast box is located below a 1780 kN-capacity load frame that supports a cyclic loading apparatus comprising

an 85 kN pneumatic actuator, a load cell, an electronic pressure regulator, a PID controller, and a function generator. The cyclic loading machine is used to deliver cyclic loading to the model tie following a sine wave with an amplitude of 10.5 kN and load extrema of 3.5 kN and 24.5 kN at a frequency of 0.8 Hz for a total of 40,000 load cycles during a given test. The applied loads give rise to minimum and maximum stresses of 57.3 kPa and 400 kPa respectively at the tie–ballast interface.

The instrumentation used to monitor the tie's behavior as it is subjected to the applied cyclic loads involves a 50 kN load cell, four linear variable displacement transducers

(LVDTs), and a data acquisition system that logs the sensors' data at a frequency of 100 Hz. The four LVDTs are placed at each corner of the tie's top surface such that its average settlement may be computed at each load cycle.

A total of thirteen ballast box tests are performed during the experimental campaign presented in this paper. Four experiments consist of testing unreinforced tie-ballast assemblies resting on the stiff, competent, fair, and soft subgrades to establish a reference behavior against which the performance of geogrid-reinforced ballast samples is compared. For each artificial subgrade, three geogrid-reinforced ballast box tests are conducted in which a single geogrid layer is embedded in the ballast bed at depths of 150 mm, 200 mm, and 250 mm below the tie's base. A summary of the experiments discussed in this study is provided in Table 4.

Results

Permanent Settlement

The tie settlement curves recorded during the unreinforced ballast box tests performed over the stiff, competent, fair, and soft subgrades are shown in Fig. 3a. The experimental data for each support condition is also represented by a power model (Eq. 1) akin to that put forward by Indraratna et al. [43, 44] in which the tie's settlement (S) is expressed as a function of the number of load cycles (N), the permanent tie deflection after the first load cycle (a), and a coefficient (b) determined from non-linear regression analysis:

$$S = a \times N^b \quad (1)$$

The results presented in Fig. 3a indicate that the subgrade's strength yields a considerable influence on the development of permanent ballast deformations and consequently of the tie's settlement, with the presence of weaker subgrades below the ballast translating into the tie experiencing greater subsidence. The settlement response of each ballast sample is characterized by a rapid accumulation of permanent vertical deformation at the onset of cyclic loading caused by ballast particles sliding and moving past one another as the initially loosely packed granular assembly rearranges into a more stable packing. The densification of the ballast layer gives rise to the formation of a tight interlock between neighboring ballast particles that are now wedged against each other. The interlock leads to an increase in the ballast layer's stiffness and correspondingly contributes to reducing the rate at which settlement builds up as the granular layer behaves in an almost elastic fashion during individual loading-unloading cycles. This trend is clearly observable in the ballast sample supported by a stiff subgrade ($\text{CBR} = \infty$) in which the tie experiences the majority of its settlement within the first 10,000 load cycles while only marginal increases in settlement occur in response to further cyclic loading. However, the presence of softer subgrades below the ballast impacts the rate at which the tie settlement develops, with the tie resting on ballast layers supported by the competent, fair, and soft subgrades experiencing 75.1%, 71.9%, and 68.7% of their respective total subsidence after 10,000 load cycles compared to 85.5% for the tie-ballast assembly supported by the stiff subgrade. The total tie settlement recorded in each sample also reflects the variations in subgrade compressibility, with the tie resting on the stiff, competent, fair, and soft subgrades experiencing a total settlement of 4.62 mm, 12.10 mm, 24.46 mm, and 35.02 mm respectively at the end of the 40,000 load cycles.

Figure 3b, c, and d displays the settlement curves of ties supported by geogrid-reinforced ballast layers resting on the competent, fair, and soft subgrades respectively. For ballast layers supported by the competent subgrade ($\text{CBR} = 25$), the tie settlement curves indicate that although the inclusion of a geogrid in the granular assembly successfully reduces the magnitude of the tie's settlement, its performance appears to be insensitive to its placement depth. The tie exhibits a similar response to cyclic loading in the three reinforced tests and experiences similar settlements regardless of the geogrid's location in the ballast bed, with the marginal discrepancies that occur between the reinforced settlement curves shown in Fig. 3b being considered to be within the range of test repeatability.

The results observed in reinforced ballast layers supported by the fair subgrade ($\text{CBR} = 13$) contrast those obtained with the competent subgrade as the geogrid's relative insensitivity

Table 4 Test summary

Test no.	CBR	Condition	Reinforcement depth (mm)
1	∞ (steel plate)	Unreinforced	N/A
2	25	Unreinforced	N/A
3		Reinforced	150
4			200
5			250
6	13	Unreinforced	N/A
7		Reinforced	150
8			200
9			250
10	5	Unreinforced	N/A
11		Reinforced	150
12			200
13			250

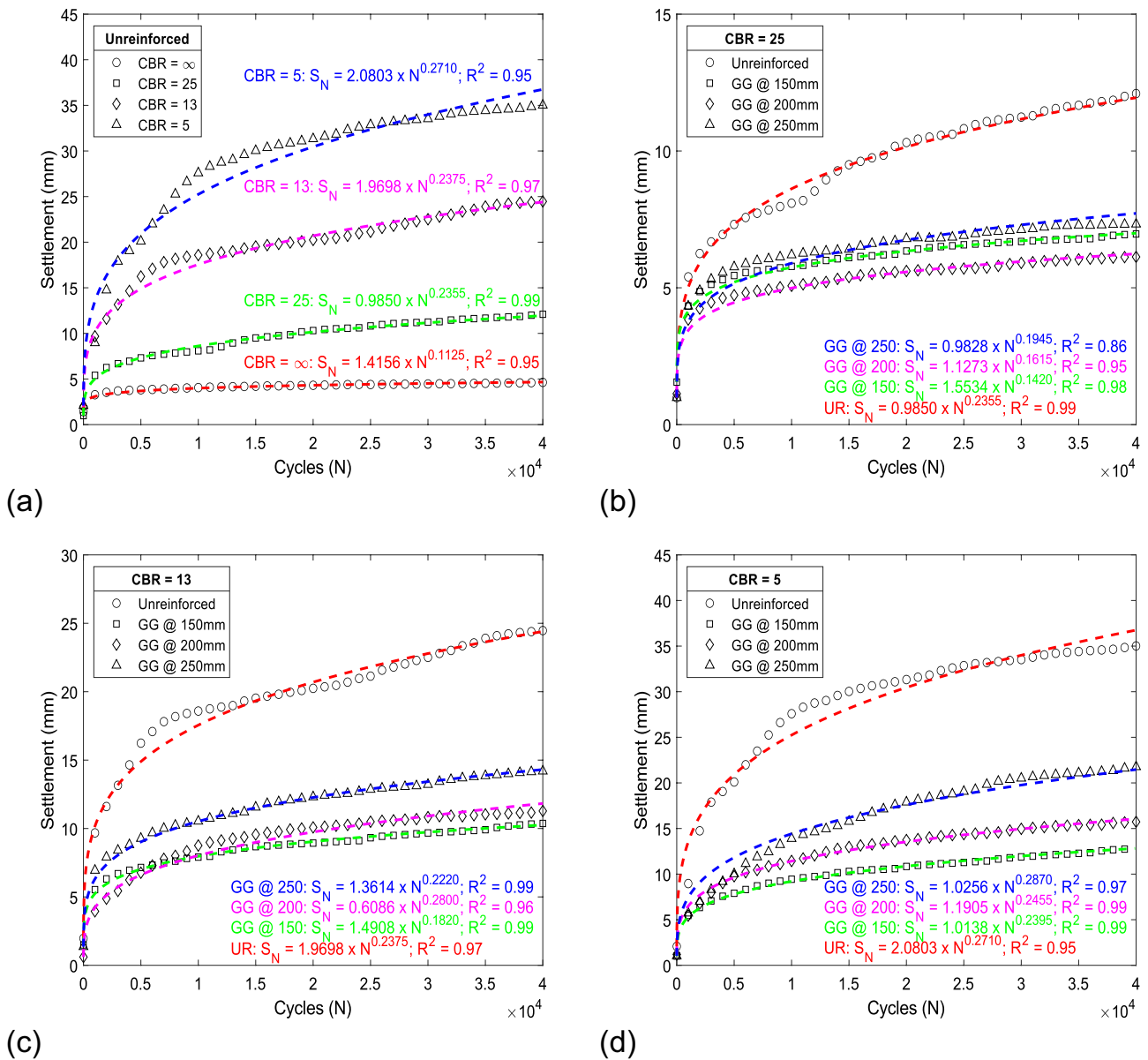


Fig. 3 Tie settlement curves recorded in **a** unreinforced ballast samples and geogrid-reinforced ballast layers supported by the **b** competent, **c** fair, and **d** soft subgrades

to its placement depth appears to vanish with the presence of a softer subgrade. Figure 3c shows the variations in tie settlement observed in geogrid-reinforced ballast beds supported by the fair subgrade. The results suggest that the ability of a geogrid to minimize tie settlement becomes sensitive to its placement depth in the ballast layer, with the geogrid placed 150 mm below the tie exhibiting a superior ability to reduce the tie’s subsidence compared to the geogrids located 200 mm and 250 mm below the tie. It is noteworthy that the geogrids placed at depths of 150 mm and 200 mm are markedly more efficient at minimizing ballast deformation than the geogrid placed deeper in the ballast layer.

The trends that materialized in geogrid-reinforced ballast beds supported by the fair subgrade are exacerbated by the presence of an even softer subgrade (i.e., soft subgrade with a CBR of 5) as shown in Fig. 3d. The tie settlement curves recorded in geogrid-reinforced ballast samples are characterized by pronounced differences that are attributed to the geogrid’s location within the ballast bed. The geogrid placed at the shallowest depth is the most effective at reducing the tie’s settlement, followed by the geogrids placed at depths of 200 mm and 250 mm respectively. The data shown in Fig. 3d highlight that as the subgrade becomes weaker, the geogrid’s location within the ballast layer becomes a key factor that

determines its ability to stabilize railroad ballast as the settlement reduction achieved by a geogrid decreases as it is located farther away from the loaded area, i.e., the tie's base.

To put the observations drawn from the results displayed in Fig. 3a–d into perspective, the settlement reduction achieved by each geogrid is represented by the settlement reduction factor (R_t) [45] computed using Eq. 2 and plotted in Figs. 4 and 5a–d.

$$R_t = 100 \times \frac{S_{UR} - S_{GG}}{S_{UR}} \quad (2)$$

where S_{UR} is the tie settlement recorded in the unreinforced ballast sample for a given subgrade and S_{GG} is the tie settlement observed in a given geogrid-reinforced ballast layer supported by the same subgrade.

The data plotted in Fig. 4 reveals that the subgrade strength wields a considerable influence on the relationship between a geogrid's placement depth and its ability to minimize ballast deformations. All geogrids placed 250 mm below the base of the tie generate similar reduction factors of approximately 40% regardless of the subgrade type. The subgrade strength starts to produce a difference in reduction factors for geogrids located at a depth of 200 mm. While the geogrid reinforcing the ballast bed supported by the competent subgrade yields a reduction factor of 41.97% that shows very little difference compared to the one obtained with a geogrid placed at 250 mm for the same subgrade, the geogrids reinforcing the ballast layers supported by the fair and soft subgrades give rise to reduction factors of 53.84%

and 57.59% respectively that correspond to increases of 4.55% and 15.19% compared to the geogrids placed at a depth of 250 mm. Similarly, geogrids placed 150 mm below the tie display a behavior that is highly sensitive to the compressibility of the underlying subgrade. As observed with the geogrid located 200 mm below the tie, the geogrid placed at a depth of 150 mm in the ballast layer supported by the competent subgrade does not yield a reduction factor that differs from those produced by the geogrids located at 250 mm, and 200 mm. On the other hand, placing the geogrid at a depth of 150 mm in the ballast bed resting on the fair subgrade results in a greater reduction factor of 55.05% compared to 53.84% and 49.29% for the geogrids located at depths of 200 mm and 250 mm. A similar, although more pronounced, trend occurs in the ballast layer supported by the soft subgrade with the geogrid placed at 150 mm resulting in a reduction factor of 63.40% compared to 57.59% and 42.40% when placed at depths of 200 mm and 250 mm respectively. Additionally, these observations are supported by Fig. 5a–d which show the reduction factors obtained in every single reinforced ballast layer after 10,000, 20,000, 30,000, and 40,000 load cycles respectively. The figures indicate that throughout the ballast box tests, the greatest reduction factors occur in ballast samples supported by the weakest subgrades reinforced with a geogrid located as close to the tie's base as possible. The figures further illustrate the influence of the subgrade's strength on a geogrid's ability to reduce ballast deformations with the geogrids placed at 150 mm and 200 mm in ballast layers supported by the fair and soft subgrades being wrapped with reduction factor contours greater than or equal to 50% throughout the entire test duration while the geogrids placed at 250 mm and those reinforcing ballast supported by the competent subgrade consistently have the lowest reduction factors.

In terms of practical implications, Figs. 4 and 5 suggest that when geogrids are used to reinforce ballast layers supported by stiff subgrades, they can be placed at the ballast–sub-ballast interface or deep within the ballast layer as their placement depth does not wield a significant influence on their ability to reinforce the granular material. On the other hand, in cases where ballast layers supported by weaker subgrades are to be reinforced with geogrids, placing the geogrids above the ballast–sub-ballast interface and closer to the tie's base is desirable as their ability to stabilize ballast is a function of their proximity to the loaded area.

Resilient Settlement

The tie's resilient settlement is defined as the difference between the tie's maximum and minimum settlements during a given load cycle and provides a measure of its elastic rebound. Figure 6a displays the variations of the tie's resilient deflection in unreinforced ballast samples resting on the

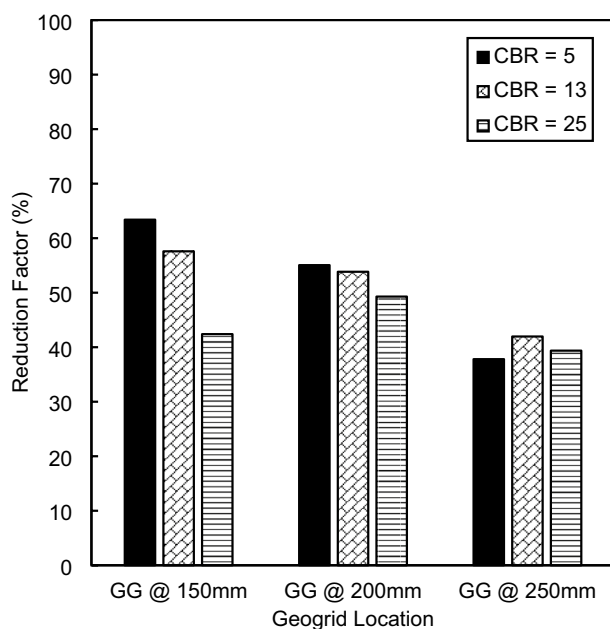


Fig. 4 Final tie settlement reduction factors in geogrid-reinforced ballast layers

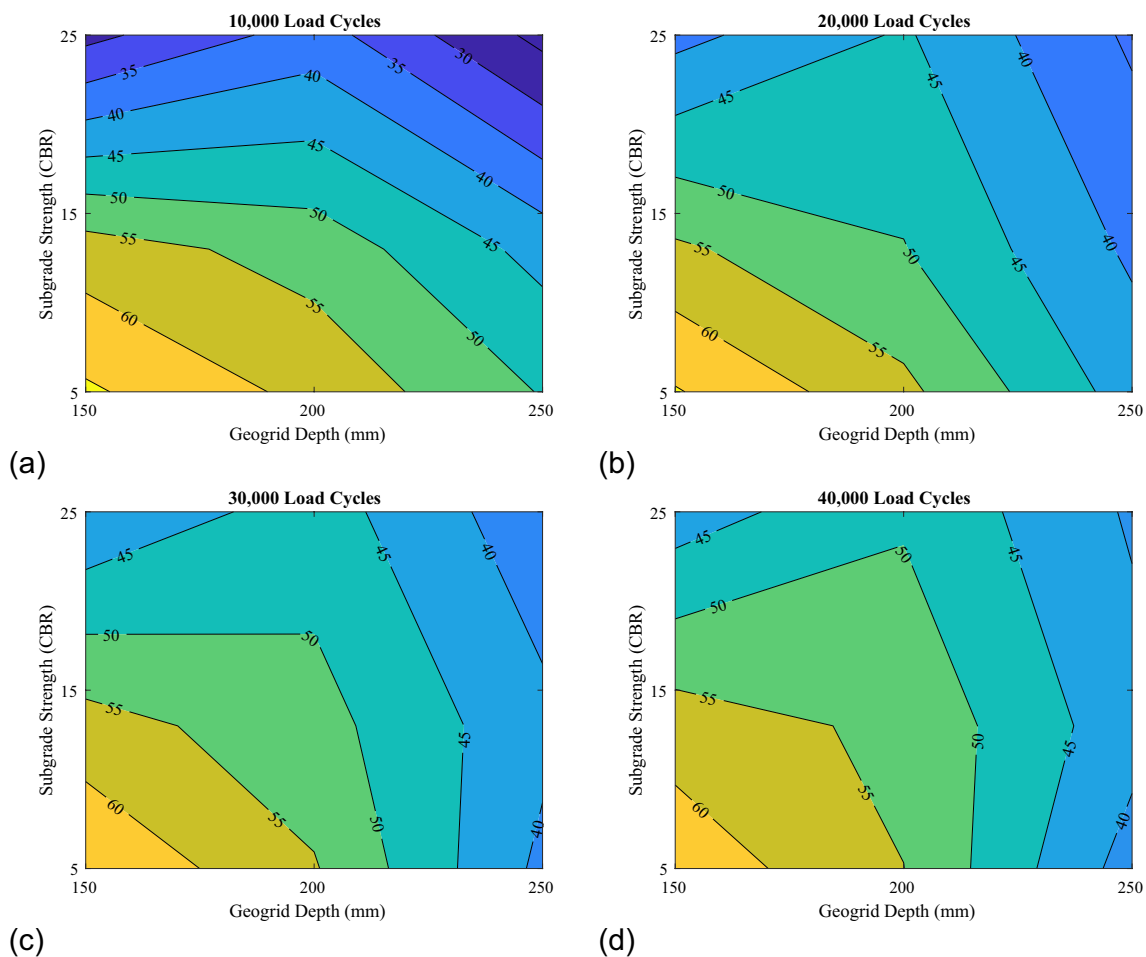


Fig. 5 Evolution of the reduction factor generated by a geogrid as a function of its placement depth and the subgrade strength after **a** 10,000, **b** 20,000, **c** 30,000, and **d** 40,000 load cycles

stiff, competent, fair, and soft subgrades. The resilient deformation is highly sensitive to changes in subgrade compressibility with the tie tested on the stiff subgrade experiencing a resilient deflection of 0.36 mm at the end of the 40,000 load cycles compared to 0.59 mm, 0.81 mm, and 0.86 mm for the competent, fair, and soft subgrades. For every subgrade, the evolution of the tie's resilient settlement follows a similar pattern whereby the tie first exhibits a high resilient deflection followed by a sharp decrease during the first 10,000 load cycles as the initially loose ballast assembly densifies under the action of repeated loads before reaching a dense stable state which manifests itself by having the resilient deformation reach a stable plateau.

Figure 6b–d shows the variations in the tie's resilient settlement recorded in unreinforced and geogrid-reinforced ballast samples supported by the competent, fair, and soft subgrades respectively. In all three figures, the inclusion of a geogrid in ballast samples is seen to translate into a reduction of the tie's resilient deformation. This reduction is attributed to the formation of a mechanical interlock between

the geogrid and the surrounding aggregate. As ballast particles become wedged in the geogrid's apertures, the ballast–geogrid interface acts as a non-displacement boundary that laterally confines the granular assembly, thereby increasing its stiffness and decreasing the recoverable settlement it experiences under cyclic loading.

The variations in tie resilient deflection recorded over the competent subgrade (Fig. 6b) reflect the findings drawn from the settlement curves for the same subgrade shown in Fig. 3b. The inclusion of a geogrid in the ballast layer minimizes the magnitude of the tie's resilient deflection throughout the entire 40,000 load cycles. However, the performance of a given geogrid appears to be marginally sensitive to its placement depth as the geogrids placed at depths of 150 mm, 200 mm, and 250 mm give rise to similar reductions in resilient settlement.

The changes in the tie's resilient settlement observed in ballast layers supported by the fair subgrade (Fig. 6c) point to the fact that a softer support condition fosters an environment in which a geogrid's placement depth becomes a

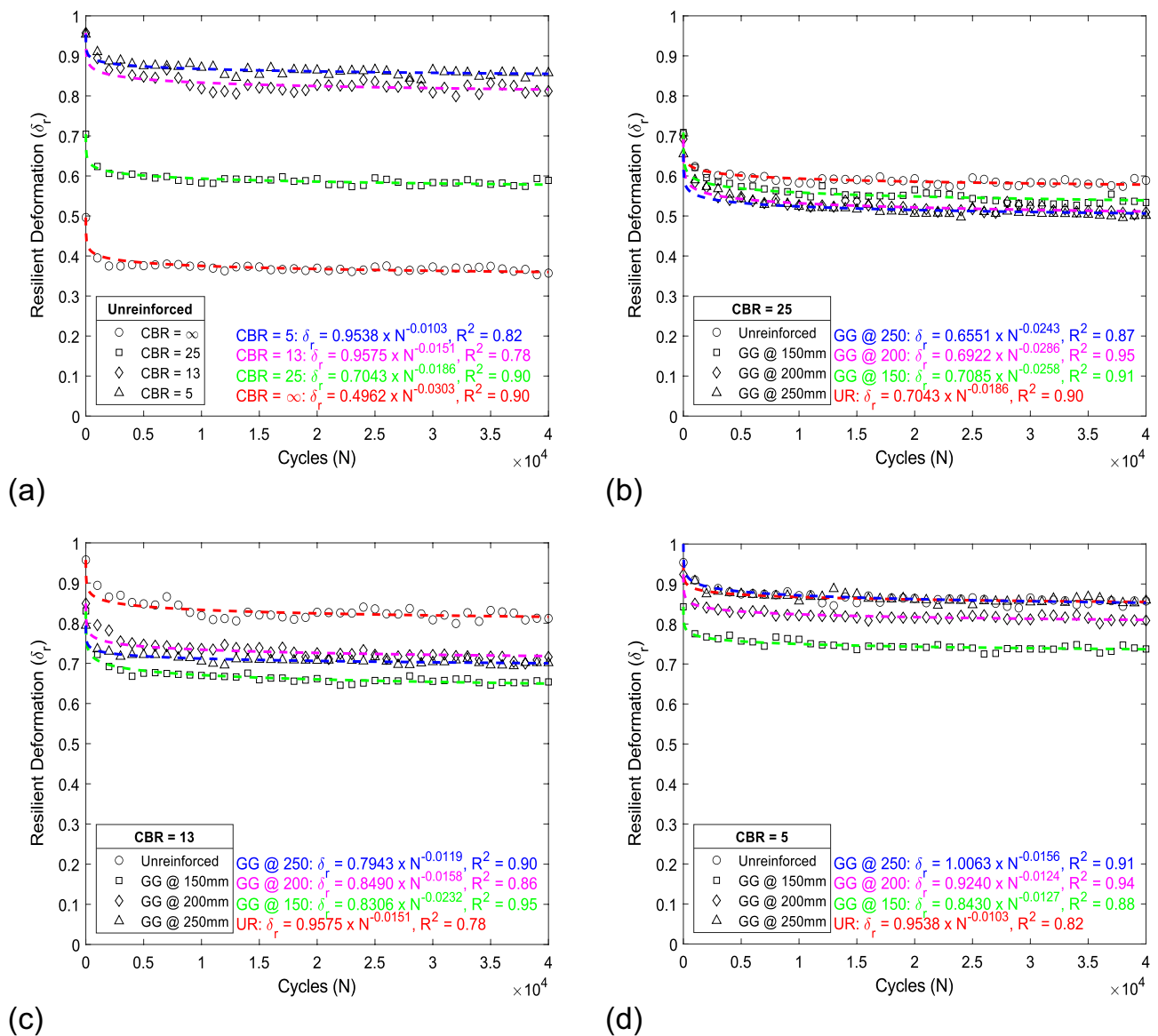


Fig. 6 Variations in the tie’s resilient deformation recorded in **a** unreinforced ballast samples and geogrid-reinforced ballast layers supported by the **b** competent, **c** fair, and **d** soft subgrades

factor that determines its ability to reinforce railroad ballast. The geogrid located 150 mm below the base of the tie achieves the greatest reduction in resilient deflection while the ones located at depths of 200 mm and 250 mm lead to a smaller decrease in resilient settlement. The observation is further substantiated by the results obtained during ballast box tests with the soft subgrade (Fig. 6d) in which a marked difference exists between the tie’s resilient deflection in ballast samples reinforced with geogrids located at different depths. The greatest reduction in resilient settlement takes place in the ballast sample reinforced with the geogrid placed 150 mm below the tie followed by the one

where the geogrid is embedded at a depth of 200 mm. It is worth noting that the geogrid located 250 mm into the ballast layer does not offer any appreciable decrease in the tie’s resilient deflection as it displays a resilient settlement curve akin to that of the unreinforced tie–ballast assembly.

Tie Support Stiffness

The tie support stiffness (K) is calculated by dividing the load amplitude (ΔP) by the tie’s resilient deflection (δ_r) during a given load cycle as shown in Eq. 3 [46–48]:

$$K = \frac{\Delta P}{\delta_r} \tag{3}$$

The evolution of the tie’s support stiffness in unreinforced ballast samples supported by the stiff, competent, fair, and soft subgrades is shown in Fig. 7a. The variations in tie support stiffness reflect the trends observed in the tie’s permanent and resilient deflections whereby the initially loose state of the ballast layer and its progressive densification and stiffening during the first 10,000 load cycles translate into the support stiffness experiencing a period of rapid increase followed by a period where it remains almost unchanged

under further cyclic loading as the denser granular assembly behaves almost elastically. Similar to the resilient deflection, the support stiffness is highly sensitive to the subgrade strength, with the highest stiffness being recorded in the ballast layer supported by the stiff subgrade followed by ballast samples resting on the competent, fair, and soft subgrades respectively.

The inclusion of geogrids in ballast layers generates an increase in the tie support stiffness owing to the development of a mechanical interlock between the geogrid and the surrounding particulate medium. As ballast particles become wedged in the grid’s apertures, the ballast layer is subjected

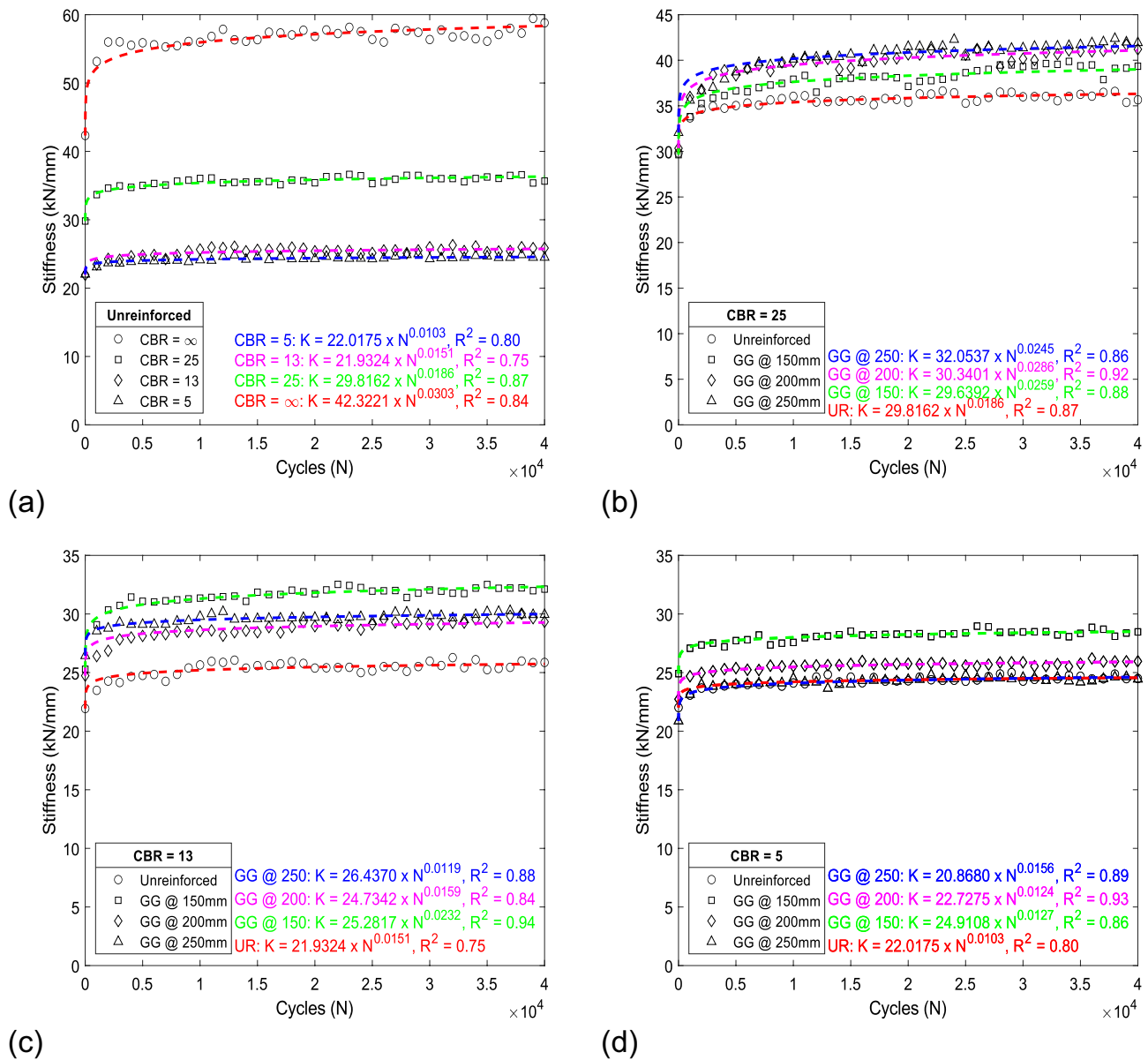


Fig. 7 Variations in tie support stiffness recorded in **a** unreinforced ballast samples and geogrid-reinforced ballast layers supported by the **b** competent, **c** fair, and **d** soft subgrades

to greater lateral confinement that minimizes the granular assembly's proclivity to deform when exposed to cyclic loading and translates into the geogrid-reinforced ballast offering a greater support stiffness to the overlying tie.

Figure 7b shows the evolution of the tie support stiffness in geogrid-reinforced and unreinforced ballast layers supported by the competent subgrade. Placing a geogrid in ballast samples results in tie support stiffnesses that consistently exceed that recorded in the unreinforced sample due to the ensuing reduced resilient deflection. However, the stiffness of geogrid-reinforced ballast supported by the competent subgrade appears to be independent of the reinforcement's location in the granular assembly, echoing the findings reported for the tie's permanent and resilient deflections.

A geogrid's propensity to increase the support stiffness of ballast assemblies becomes increasingly tied to its placement depth as the strength of the underlying subgrade decreases. The support stiffnesses observed in geogrid-reinforced and unreinforced ballast layers supported by the fair subgrade are displayed in Fig. 7c. Although all reinforced ballast layers have higher stiffness than the unreinforced ballast sample, a notable difference exists between the ballast assembly reinforced with a geogrid located 150 mm below the tie and those where the geogrid is at depths of 200 mm and 250 mm. Specifically, the ballast layer with a geogrid placed at a depth of 150 mm has a greater stiffness compared to the other two layers that exhibit similar stiffnesses. The observation that the subgrade strength plays a role in determining whether the geogrid's location wields an influence on its impact on the ballast stiffness is further substantiated by the variations in support stiffness in unreinforced and geogrid-reinforced ballast layers resting on the soft subgrade shown in Fig. 7d. The ballast layer reinforced with a geogrid placed at a depth of 150 mm experiences the greatest stiffness increase of all the reinforced samples, culminating in a stiffness that is 16.3% higher than that of the unreinforced sample at the end of the test. The ballast sample reinforced with a geogrid placed at a depth of 200 mm develops a smaller increase in its support stiffness, resulting in a stiffness that is 6% greater than in the unreinforced case at the end of the test. In contrast, placing a geogrid 250 mm below the tie does not appear to affect the support stiffness, as the ensuing stiffness is akin to that obtained in the unreinforced ballast layer.

Damping Ratio

Railroad ballast exhibits a hysteretic behavior when subjected to cyclic loading which is characterized by the storage and dissipation of energy during a given loading–unloading cycle. In the experiments presented herein, the energy dissipation in railroad ballast stems from the plastic rearrangement of the soil fabric that takes place as individual ballast particles rearrange in response to the application of external

loads. The ballast's propensity to dissipate energy during cyclic loading is examined experimentally by analyzing the hysteresis loops generated during a given ballast box test to compute the damping ratio (D_r) for each load cycle using Eq. 4 as per ASTM D3999 [49]:

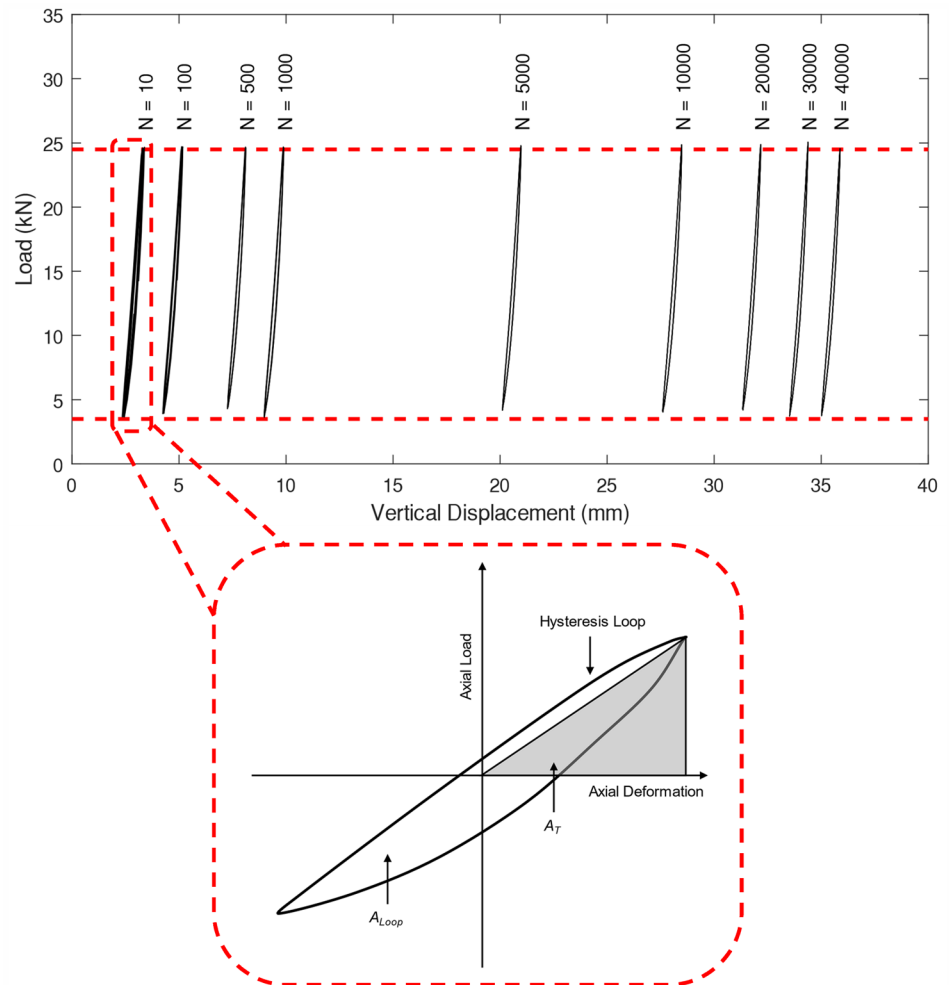
$$D_r = \frac{A_{\text{Loop}}}{4\pi A_T} \quad (4)$$

where A_{Loop} is the area bounded by the hysteresis loop for a given cycle and A_T is the area contained within the shaded triangle shown in Fig. 8. The area contained within a given hysteresis loop provides a measure of the energy dissipated by the material during a given load cycle while the shaded triangle represents the maximum elastic energy that may be stored per unit volume of the material. It is important to emphasize that the damping ratios calculated in this paper are a function of the ballast's properties (as well as any geogrid inclusion that may be embedded in it) and the underlying subgrade.

Figure 9a displays the variations in damping ratio in unreinforced ballast samples tested over the stiff, competent, fair, and soft subgrades. In general, the damping ratio of a given test initially has a high value at the beginning of a test and experiences a sharp drop within the first 10,000 load cycles followed by a stage where it decreases at a much lower rate. This echoes the observations made in Figs. 3a and 6a where the onset of cyclic loading consistently leads to either the settlement or resilient deflection varying significantly due to the plastic rearrangement of the ballast's fabric followed by either property varying in a more stable fashion. The damping ratios of the unreinforced tie–ballast assemblies exhibit a strong sensitivity to the presence of a compressible subgrade with the damping ratio over the stiff subgrade reaching a value of 0.029 at the end of the ballast box test against 0.071, 0.074, and 0.078 in unreinforced experiments performed over the competent, fair, and soft subgrades respectively.

The inclusion of geogrid reinforcement in ballast layers supported by the competent subgrade results in a small reduction in damping ratio compared to the unreinforced case as shown in Fig. 9b, with only minor differences in damping ratio being recorded between each reinforced test. However, the experiments performed in reinforced ballast samples supported by the fair and soft subgrades (Fig. 9c and d respectively) indicate that negligible reductions in damping ratio occur as a consequence of reinforcing railroad ballast with a geogrid, regardless of its placement depth. Bearing in mind that the results displayed in Fig. 9a–d are a reflection of the ballast/subgrade assembly's propensity to dissipate energy during cyclic loading, the data suggests that a geogrid only generates marginal reductions in the damping ratio and that the energy dissipated by the ballast/subgrade assembly is mainly a function of the subgrade's strength.

Fig. 8 Hysteresis loops recorded during the ballast box test performed on the unreinforced tie–ballast assembly supported by the soft subgrade and the areas used to evaluate its damping ratio



Limitations

The results presented in this paper are influenced by the fact that elastomer pads were used to simulate the presence of different subgrades below the tie–ballast assembly. Unlike natural soils, the rubber mats may not sustain permanent plastic deformations under cyclic loading. As such, while they provided different degrees of resiliency to the overlying ballast which allowed the granular material to exhibit different deformation behaviors, the pads' response to cyclic loading remained the same throughout the experiments and may not fully represent the behavior of natural subgrades. It is noteworthy that the loading frequency and the relatively low number of load cycles used in the ballast box tests may not be an actual representation of typical train traffic loading while the box's rigid boundaries may not allow for the physical modeling of low levels of lateral confinement. Additionally, the impact of geogrid inclusions on the ballast suffusion potential should be assessed. The detachment and transport of fine particles within railroad ballast may potentially induce internal instability in the ballast layer [50].

Hence, additional research is necessary to investigate how geogrids influence the potential for suffusion in reinforced ballast samples.

Conclusions

This study focuses on evaluating the effect of the subgrade strength on the ability of geogrids to reinforce railroad ballast when placed at different locations below the tie. To do so, a total of thirteen ballast box tests are conducted on unreinforced and geogrid-reinforced ballast samples subjected to cyclic loading. The key findings of the experimental campaign are as follows:

- The subgrade strength wields a considerable influence on the type of reinforcement benefit derived from embedding a geogrid in railroad ballast
- For ballast layers supported by a competent subgrade, the use of geogrid reinforcement leads to a reduction in tie

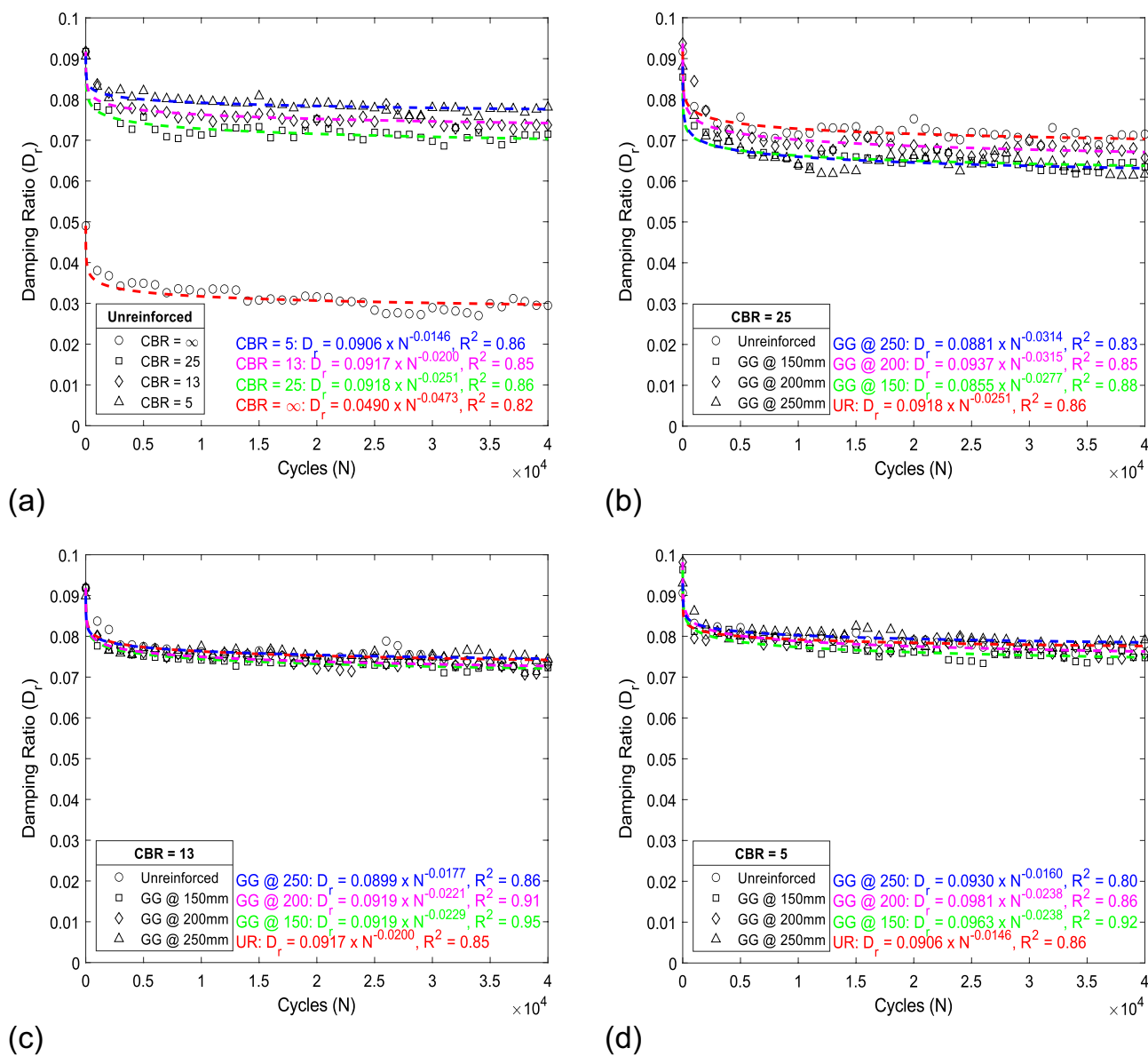


Fig. 9 Evolution of the ballast-subgrade assembly’s damping ratio recorded in **a** unreinforced ballast samples and geogrid-reinforced ballast layers supported by the **b** competent, **c** fair, and **d** soft subgrades

settlement that remains relatively the same regardless of the geogrid’s placement depth

- A geogrid’s placement depth becomes increasingly important when the reinforced ballast layer rests on the fair or soft subgrade, with geogrids located closer to the tie being more effective at minimizing the tie’s settlement. While this trend is observable in reinforced ballast samples supported by the fair subgrade, the effect of the geogrid’s location is particularly pronounced in reinforced tie–ballast assemblies resting on the soft subgrade
- The reductions in resilient settlement produced by geogrids follow the trends observed for the tie’s permanent settlement whereby geogrid-reinforced ballast layers

resting on a competent subgrade display similar resilient deformations regardless of the reinforcement’s location while reinforced tie–ballast assemblies supported by weaker subgrades exhibit reductions in resilient deformation that are strongly influenced by the geogrid’s location, with shallower placement depths resulting in the greatest reductions

- Embedding a geogrid in a ballast layer enhances the track support stiffness. For ballast layers resting on the competent subgrade, the geogrid location appears to have a marginal impact on the ensuing increase in stiffness. The geogrid’s placement depth becomes increasingly important, however, when the strength of the underlying

subgrade decreases, with geogrids located closer to the bottom of the tie leading to greater stiffness increases compared to those situated deeper within the ballast layer

- The damping ratio appears to be relatively insensitive to the presence of geogrid reinforcement with only minor differences in damping being observed between unreinforced and geogrid-reinforced tie–ballast assemblies. The damping ratio is primarily affected by the strength of the underlying subgrade

Acknowledgements The authors are grateful for Dr. William Cook, Mr. John Bartczak, and Mr. Mike Stephens of the Jamieson Structures Laboratory at McGill University whose assistance throughout the experimental campaign was extremely valuable.

Author Contributions RLED: Conceptualization, methodology, investigation, formal analysis, visualization, resources, writing—original draft. MAM: Funding acquisition, resources, supervision, writing—review and editing. SB: Funding acquisition, resources, writing—review and editing.

Funding This research is funded by an NSERC Alliance grant (NSERC ALLRP 5617) in partnership with Titan Environmental Ltd. and by the McGill Engineering Vadasz Doctoral Fellowship sponsored by the Vadasz Family Foundation.

Data Availability The data that supports the findings of this study are available upon request from the corresponding author.

Declarations

Conflict of interest The authors have no competing interests to declare that are relevant to the content of this article.

References

- Fischer S (2022) Geogrid reinforcement of ballasted railway superstructure for stabilization of the railway track geometry—a case study. *Geotext Geomembr* 50:1036–1051. <https://doi.org/10.1016/j.geotexmem.2022.05.005>
- Desbrousses RLE, Meguid MA (2021) On the analysis and design of reinforced railway embankments in cold climate: a review. In: Tighe S, Walbridge S, Henderson V (eds) CSCE 2021 Annual Conference. Springer, Niagara Falls, ON, Canada, pp 588–598
- Desbrousses RLE, Meguid MA (2022) Effect of subgrade compressibility on the reinforcing performance of railroad geogrids: insights from finite element analysis. In: GeoCalgary 2022. Canadian Geotechnical Society, Calgary, AB
- Indraratna B, Salim W, Rujikiatkamjorn C (2011) *Advanced rail geotechnology—ballasted track*. CRC Press, Leiden
- Selig ET, Sluz A (1978) Ballast and subgrade response to train loads. *Transportation Research Board*, no 694, pp 53–60. ISSN: 0361-1981
- Selig ET, Waters JM (1994) *Track geotechnology and substructure management*. Thomas Telford Ltd, London
- Indraratna B, Lackenby J, Christie D (2005) Effect of confining pressure on the degradation of ballast under cyclic loading. *Géotechnique* 55:325–328. <https://doi.org/10.1680/geot.2005.55.4.325>
- Lackenby J, Indraratna B, McDowell G, Christie D (2007) Effect of confining pressure on ballast degradation and deformation under cyclic triaxial loading. *Géotechnique* 57:527–536. <https://doi.org/10.1680/geot.2007.57.6.527>
- Thakur PK, Vinod JS, Indraratna B (2013) Effect of confining pressure and frequency on the deformation of ballast. *Geotechnique* 63:786–790. <https://doi.org/10.1680/geot.12.T.001>
- Sun Q, Indraratna B, Nimbalkar S (2014) Effect of cyclic loading frequency on the permanent deformation and degradation of railway ballast. *Geotechnique* 64:746–751. <https://doi.org/10.1680/geot.14.T.015>
- Sun Q, Indraratna B, Ngo NT (2019) Effect of increase in load and frequency on the resilience of railway ballast. *Geotechnique* 69:833–840. <https://doi.org/10.1680/jgeot.17.P.302>
- Sussmann TR, Ruel M, Chrismer SM (2012) Source of ballast fouling and influence considerations for condition assessment criteria. *Transp Res Rec J Transp Res Board* 2289:87–94. <https://doi.org/10.3141/2289-12>
- Bruzek R, Stark TD, Wilk ST et al (2016) Fouled ballast definitions and parameters. In: 2016 Joint rail conference. American Society of Mechanical Engineers
- Malisetty RS, Indraratna B, Qi Y, Rujikiatkamjorn C (2022) Shakedown response of recycled rubber-granular waste mixtures under cyclic loading. *Geotechnique*. <https://doi.org/10.1680/jgeot.21.00040>
- Li D, Hyslip J, Sussmann T, Chrismer S (2015) *Railway geotechnics*. CRC Press, London
- Kashani HF, Hyslip JP, Ho CL (2017) Laboratory evaluation of railroad ballast behavior under heavy axle load and high traffic conditions. *Transp Geotech* 11:69–81. <https://doi.org/10.1016/j.trgeo.2017.04.002>
- Faghihi Kashani H, Ho CL, Hyslip JP (2018) Fouling and water content influence on the ballast deformation properties. *Constr Build Mater* 190:881–895. <https://doi.org/10.1016/j.conbuildmat.2018.09.058>
- Chrismer S, Davis D (2000) Cost comparisons of remedial methods to correct track substructure instability. *Transp Res Rec*. <https://doi.org/10.3141/1713-02>
- Touqan M, Ahmed A, El Naggar H, Stark T (2020) Static and cyclic characterization of fouled railroad sub-ballast layer behaviour. *Soil Dyn Earthq Eng* 137:106293. <https://doi.org/10.1016/j.soildyn.2020.106293>
- Anderson WF, Key AJ (2000) Model testing of two-layer railway track ballast. *J Geotech Geoenvironmental Eng* 126:317–323. [https://doi.org/10.1061/\(ASCE\)1090-0241\(2000\)126:4\(317\)](https://doi.org/10.1061/(ASCE)1090-0241(2000)126:4(317))
- Sol-Sánchez M, Moreno-Navarro F, Rubio-Gámez MC (2016) Analysis of ballast tamping and stone-blowing processes on railway track behaviour: the influence of using USPs. *Geotechnique* 66:481–489. <https://doi.org/10.1680/jgeot.15.P.129>
- D'Angelo G, Sol-Sanchez M, Moreno-Navarro F et al (2018) Use of bitumen-stabilised ballast for improving railway trackbed conventional maintenance. *Geotechnique* 68:518–527. <https://doi.org/10.1680/jgeot.17.P.022>
- Prasad KVS, Hussaini SKK (2022) Review of different stabilization techniques adapted in ballasted tracks. *Constr Build Mater* 340:127747. <https://doi.org/10.1016/j.conbuildmat.2022.127747>
- Luo Z, Zhao C, Cai W et al (2023) Full-scale model tests on ballasted tracks with/without geogrid-stabilization under high-speed train loads. *Géotechnique* 19(6):1–43. <https://doi.org/10.1680/jgeot.22.00339>
- Marx DH, Kumar K, Zornberg JG (2023) Quantification of geogrid lateral restraint using transparent sand and deep learning-based image segmentation. *Geotext Geomembr*. <https://doi.org/10.1016/j.geotexmem.2023.04.004>
- Indraratna B, Ngo NT, Rujikiatkamjorn C (2011) Behavior of geogrid-reinforced ballast under various levels of fouling. *Geotext Geomembr* 29:313–322. <https://doi.org/10.1016/j.geotexmem.2011.01.015>

27. Indraratna B, Karimullah Hussaini SK, Vinod JS (2012) On the shear behavior of ballast-geosynthetic interfaces. *Geotech Test J* 35:103317. <https://doi.org/10.1520/GTJ103317>
28. Indraratna B, Hussaini SKK, Vinod JS (2013) The lateral displacement response of geogrid-reinforced ballast under cyclic loading. *Geotext Geomembr* 39:20–29. <https://doi.org/10.1016/j.geotexmem.2013.07.007>
29. Hussaini SKK, Indraratna B, Vinod JS (2015) Performance assessment of geogrid-reinforced railroad ballast during cyclic loading. *Transp Geotech* 2:99–107. <https://doi.org/10.1016/j.trgeo.2014.11.002>
30. Hussaini SKK, Indraratna B, Vinod JS (2016) A laboratory investigation to assess the functioning of railway ballast with and without geogrids. *Transp Geotech* 6:45–54. <https://doi.org/10.1016/j.trgeo.2016.02.001>
31. Sweta K, Hussaini SKK (2019) Behavior evaluation of geogrid-reinforced ballast-subballast interface under shear condition. *Geotext Geomembranes* 47:23–31. <https://doi.org/10.1016/j.geotexmem.2018.09.002>
32. Hussaini SKK, Sweta K (2020) Application of geogrids in stabilizing rail track substructure. *Front Built Environ* 6:1–13. <https://doi.org/10.3389/fbuil.2020.00020>
33. Sweta K, Hussaini SKK (2020) Effect of geogrid on deformation response and resilient modulus of railroad ballast under cyclic loading. *Constr Build Mater* 264:120690. <https://doi.org/10.1016/j.conbuildmat.2020.120690>
34. Sweta K, Hussaini SKK (2022) Role of particle breakage on damping, resiliency and service life of geogrid-reinforced ballasted tracks. *Transp Geotech* 37:100828. <https://doi.org/10.1016/j.trgeo.2022.100828>
35. Brown SF, Kwan J, Thom NH (2007) Identifying the key parameters that influence geogrid reinforcement of railway ballast. *Geotext Geomembr* 25:326–335. <https://doi.org/10.1016/j.geotexmem.2007.06.003>
36. Bathurst RJ, Raymond GP (1987) Geogrid reinforcement of ballasted track. *Transportation Research Record*, no 1153, pp 8–14. ISSN: 0361-1981
37. Bathurst RJ, Raymond GP, Jarrett PM (1986) Performance of geogrid-reinforced ballast railroad track support. In: *Third international conference on geotextiles*. Vienna, Austria, pp 43–48
38. Yu Z, Woodward PK, Laghrouche O, Connolly DP (2019) True triaxial testing of geogrid for high speed railways. *Transp Geotech* 20:100247. <https://doi.org/10.1016/j.trgeo.2019.100247>
39. AREMA (2010) *Manual for railway engineering*. AREMA, Lanham
40. Desbrousses RLE, Meguid MA, Bhat S (2021) Effect of temperature on the mechanical properties of two polymeric geogrid materials. *Geosynth Int*. <https://doi.org/10.1680/jgein.21.00032a>
41. Titan Environmental Containment (2023) Titan Rail Grid 30: Biaxial Polypropylene Geogrid Specifications Sheet. <https://titanenviro.com/wp-content/uploads/2023/09/Titan-Rail-Grid-30.pdf>
42. ASTM (2005) ASTM D1883–07: standard test method for CBR (California bearing ratio) of soils in place. *ASTM Stand Guid* 04:21–24. <https://doi.org/10.1520/D1883-21>
43. Indraratna B, Ionescu D, Christie HD (2000) State-of-the-art large scale testing of ballast. In: *Conf Railw Eng* 21–23 May 2000, pp 208–220
44. Indraratna B, Khabbaz H, Salim W, Christie D (2006) Geotechnical properties of ballast and the role of geosynthetics in rail track stabilisation. *Proc Inst Civ Eng Gr Improv* 10:91–101. <https://doi.org/10.1680/grim.2006.10.3.91>
45. Shin EC, Kim DH, Das BM (2002) Geogrid-reinforced railroad bed settlement due to cyclic load. *Geotech Geol Eng* 20:261–271. <https://doi.org/10.1023/A:1016040414725>
46. Shi C, Zhao C, Yang Y et al (2021) Analysis of railway ballasted track stiffness and behavior with a hybrid discrete-continuum approach. *Int J Geomech* 21:1–10. [https://doi.org/10.1061/\(asce\)gm.1943-5622.0001941](https://doi.org/10.1061/(asce)gm.1943-5622.0001941)
47. Grossoni I, Andrade AR, Bezin Y (2016) Assessing the role of longitudinal variability of vertical track stiffness in the long-term deterioration. In: *Dyn Veh Roads Tracks—Proc 24th Symp Int Assoc Veh Syst Dyn IAVSD 2015*, pp 851–860. <https://doi.org/10.1201/b21185-91>
48. Abadi T, Le PL, Zervos A, Powrie W (2018) Improving the performance of railway tracks through ballast interventions. *Proc Inst Mech Eng Part F J Rail Rapid Transit* 232:337–355. <https://doi.org/10.1177/0954409716671545>
49. ASTM (1996) ASTM D3999–91 standard test methods for the determination of the modulus and damping properties of soils using the cyclic triaxial apparatus. *Annu B ASTM Stand*. <https://doi.org/10.1520/D3999-11>
50. Liu K, Qiu R, Su Q et al (2021) Suffusion response of well graded gravels in roadbed of non-ballasted high speed railway. *Constr Build Mater* 284:122848. <https://doi.org/10.1016/j.conbuildmat.2021.122848>

Publisher's Note Springer Nature remains neutral with regard to jurisdictional claims in published maps and institutional affiliations.

Springer Nature or its licensor (e.g. a society or other partner) holds exclusive rights to this article under a publishing agreement with the author(s) or other rightsholder(s); author self-archiving of the accepted manuscript version of this article is solely governed by the terms of such publishing agreement and applicable law.